Nano Research 2017, 10(5): 1651–1661
DOI 10.1007/s12274-016-1377-2
Research Article
ISSN 1998-0124
CN 11-5974/O4

A pH-switched mesoporous nanoreactor for synergetic therapy

Zhengqing Yan[1,2], Andong Zhao[1,2], Xinping Liu[1,2], Jinsong Ren[1], and Xiaogang Qu[1] (✉)

[1] *Laboratory of Chemical Biology and State Key Laboratory of Rare Earth Resource Utilization, Changchun Institute of Applied Chemistry, Chinese Academy of Sciences, Changchun 130022, China*
[2] *University of Chinese Academy of Sciences, Beijing 100039, China*

Received: 9 September 2016
Revised: 8 November 2016
Accepted: 15 November 2016

KEYWORDS
zinc oxide,
mesoporous nanoreactor,
non-specific degradation,
controllable release,
fluorescent imaging

ABSTRACT

Zinc oxide nanoparticles (ZnO NPs), as a new type of pH-sensitive drug carrier, have received much attention. ZnO NPs are stable at physiological pH, but can dissolve quickly in the acidic tumor environment (pH < 6) to generate cytotoxic zinc ions and reactive oxygen species (ROS). However, the protein corona usually causes the non-specific degradation of ZnO NPs, which has limited their application considerably. Herein, a new type of pH-sensitive nanoreactor (ZnO-DOX@F-mSiO_2-FA), aimed at reducing the non-specific degradation of ZnO NPs, is presented. In the acidic tumor environment (pH < 6), it can release cytotoxic zinc ions, ROS, and anticancer drugs to kill cancer cells effectively. In addition, the fluorescence emitted from fluorescein isothiocyanate (FITC)-labeled mesoporous silica (F-mSiO_2) and doxorubicin (DOX) can be used to monitor the release behavior of the anticancer drug. This report provides a new method to avoid the non-specific degradation of ZnO NPs, resulting in synergetic therapy by taking advantage of ZnO NPs-induced oxidative stress and targeted drug release.

1 Introduction

Over the last decade, the development of nanometer-sized drug carriers for targeted delivery and controllable release has become one of the most promising fields in biomedicine. In particular, the controllable release of therapeutic agents not only maintains suitable drug levels within the therapeutic window, but also maximizes therapeutic efficiency to avoid unwanted side effects [1–5]. Therefore, different controllable drug carriers have been engineered in response to various external stimuli, such as pH, temperature, light, ionic strength, redox reagents, and enzymes [6–10]. The pH value in the tumor microenvironment is lower than that in blood and normal tissues; therefore, the pH-controlled release of anticancer drugs is of great benefit to cancer treatment [11–13]. Thus, pH-responsive materials (pH-sensitive linker, pH-responsive polymer micelles, and pH-tunable calcium phosphate) are generally used to construct pH-responsive drug carriers.

Address correspondence to xqu@ciac.ac.cn

Although promising, these materials usually need harsh pH environments (pH 3–4 or pH 10), which hinders their further application [6–7, 14]. Thus, there is an urgent need to develop more effective pH-responsive drug carriers. Zinc oxide nanoparticles (ZnO NPs), as a new type of pH-sensitive material, have attracted much attention [15–20].

ZnO NPs are usually stable at physiological pH (pH 7.4), while they can dissolve quickly under the acid tumor environment (pH < 6) to generate cytotoxic zinc ions and reactive oxygen species (ROS), which can kill cancer cells effectively [21–25]. In addition, the interaction of ZnO NPs with doxorubicin (DOX) can significantly change the spectrum of DOX, which can then be used to monitor DOX release behavior [26–28]. These advantages make ZnO NPs promising candidates for pH-responsive drug carriers. However, before ZnO NPs reach the target sites, many proteins in the serum will adsorb onto the surface of the ZnO NPS, resulting in the formation of a protein corona. Subsequently, the protein corona can increase the non-specific degradation rates of ZnO NPs because of aqueous complex formation and ligand-enhanced dissolution mechanisms [29–32]. Inevitably, the released zinc ions and ROS produced by ZnO NPs will lead to damage to adjacent normal cells.

Although surface modifications such as PEGylation and iron-doping methods have been used to reduce the side effects of ZnO NPs caused by the protein corona, both the ZnO degradation rate and the efficiency of cancer cell killing decrease at the same time [33, 34]. Thus, it remains necessary to develop an effective ZnO NPs-based drug carrier for cancer therapy. Mesoporous silica-based nanoreactors might represent one solution to this problem [35]. These nanoreactors can control substance exchange and can compartmentalize different regions to avoid unnecessary chemical reactions. For example, Correa-Duarte and his colleagues reported that a mesoporous silica nanoreactor could be used to induce confined chemical reactions thermally [36]. Our group has developed an efficient nanoreactor to achieve reversible pH-regulation based on enzymatic reactions [37]. Moreover, pH-responsive drug carriers have been developed based on mesoporous silica nanoreactors [38–42]. Mesoporous silica materials have distinctive advantages, including biocompatibility, tunable pores, large load capacity, and the ability to functionalize their surfaces [43–46]; thus, they can be modified readily by fluorescent probes and target molecules. In addition, it is important to monitor drug release behavior for drug carriers, which is helpful to evaluate drug efficacy [47–51]. Considering the complexity of the tumor environment, large volume of non-specific signals usually result in a poor target-to-background signal ratio. Therefore, two-fluorescence imaging, which has been used as a fluorescent sensor [52–54], is utilized to monitor drug release.

Herein, combining the advantages of mesoporous silica nanoreactors and two-fluorescence imaging, a multifunctional drug carrier was developed to effectively protect ZnO NPs from non-specific degradation. Firstly, ZnO NPs were mixed with DOX to form a ZnO-DOX complex. This complex was then coated with fluorescein isothiocyanate (FITC)-labeled mesoporous silica (F-mSiO_2). The two fluorescent molecules (DOX and FITC) could then be used to monitor the drug release behavior. To improve the efficiency of target delivery, folate (FA) was linked on the surface of the mesoporous silica shell. This pH-sensitive drug carrier is expected to reduce the side effects of ZnO NPs caused by the protein corona and result in synergetic therapy of anticancer drugs and nanoparticle-induced oxidative stress.

2 Experimental

2.1 Preparation of ZnO@F-mSiO_2-FA or ZnO-DOX@F-mSiO_2-FA

FITC (2 mg) was reacted with 44 μL of (3-aminopropyl)triethoxysilane (APTES) in 1 mL of ethanol overnight in the dark. ZnO or ZnO-DOX (2 mg) was first dissolved in 20 mL of ethanol solution, including polyvinylpyrrolidone (PVP)-10, followed by adding 500 μL ammonium hydroxide; tetraethyl orthosilicate (TEOS) (100 μL) was then added drop wise. The APTES-modified dye solution (50 μL) was then added drop wise while stirring was continued. The mixture was allowed to ultrasonic for 4 h. Then, FA (5 mg), EDC (2.4 mg) and NHS (2 mg) were dissolved in 4-morpholineethanesulfonic acid (MES) buffer (6 mL,

pH 6.0). Next, 2 mg of the above NPs dispersion was added drop wise. The reaction mixture was incubated with agitation overnight.

2.2 Inhibiting the non-specific degradation of ZnO NPs

ZnO-DOX and ZnO-DOX@F-mSiO$_2$-FA (1 mg) NPs were dispersed in 1 mL of aqueous buffer solutions (pH 7.4 phosphate buffered saline (PBS), pH 7.4 PBS plus bovine serum albumin (BSA), and pH 4.5 acetate buffer) at 37 ℃ for 4 h, respectively. After centrifugation, the supernatant was treated with nitrohydrochloric acid to remove the BSA. The zinc ions in the supernatant were monitored by inductively coupled plasma mass spectrometry (ICP-MS).

2.3 Visualizing drug release

HeLa and HEK 293T cells were seeded at a density of 5000 cells per well (500 μL total volume/well) in 24-well assay plates and incubated for 24 h. A suspension of ZnO-DOX@F-mSiO$_2$-FA was introduced into the culture medium for 4 h, and then, free NPs were removed. A further incubation for 30 min in Hoechst stain was performed to stain the nuclei of cancer cells specifically. Finally, the cells were washed three times with PBS and examined by confocal laser scanning microscopy (CLSM).

3 Results and discussion

3.1 Preparation and characterization of pH-sensitive nanoreactors

The synthesis of our designed pH-responsive nanoreactors is illustrated in Fig. 1(a). The nanoreactors were obtained in three steps, including the formation of the ZnO-DOX complex, surface coating with F-mSiO$_2$, and then with FA. First, ZnO NPs were synthesized successfully using a solvothermal method [55]. The scanning electron microscopy (SEM) image showed that the prepared shuttle-like ZnO NPs were uniform and monodisperse, with an average length of 150 nm and a width of 100 nm (Fig. S1(a) in the Electronic Supplementary Material (ESM)). The transmission electron microscopy (TEM) image suggested that the ZnO NPs had higher surface-to-volume ratios, which made them suitable as drug carriers (Fig. S1(b) in the ESM). The X-ray diffraction (XRD) pattern of the ZnO NPs confirmed their hexagonal crystal structure (Fig. S1(c) in the ESM). ZnO and DOX were then mixed together to form the ZnO-DOX complex, which was confirmed by UV/Vis spectroscopy. As shown in Fig. S2 (in the ESM), the characteristic absorption band of DOX became red-shifted and the corresponding solution turned purple. Next, monodispersed ZnO-DOX, as a core, was modified with mesoporous silica layer using a sol–gel method and the surface of the mesoporous silica was modified with both FITC and APTES (ZnO-DOX@F-mSiO$_2$). Finally, the prepared NPs were conjugated with FA via an EDC/NHS reaction (ZnO-DOX@F-mSiO$_2$-FA). The processes were monitored by Fourier transform infrared spectrophotometry (FT-IR). As shown in Fig. S3(a) (in the ESM), the emerging absorption bands at around 1,691 and 1,606 cm^{-1} were the characteristic bands of FA, which suggested that FA was linked to the mesoporous silica shell successfully [56, 57]. Additionally, the processes were also tracked by zeta potential measurements in deionized water. As shown in Fig. S3(b) (in the ESM), the zeta potential of the original ZnO-DOX@mSiO$_2$ was –23.70 mV and increased to +19.19 mV upon amino modification. After FA-modification, the zeta potential decreased to –28.00 mV. The monodisperse and core–shell structure of the ZnO-DOX@F-mSiO$_2$-FA NPs were characterized by SEM and TEM, respectively (Figure S4(a) and S4(b) in the ESM). To further investigate the distribution of Zn and Si, elemental analysis was performed using high-angle annular dark-field SEM. The inset images of Fig. S4(b) in the ESM show the energy dispersive X-ray (EDX) elemental mapping images of Si, Zn, and N for a ZnO-DOX@F-mSiO$_2$-FA NP, further demonstrating the successful preparation of the pH-sensitive nanoreactors.

3.2 Inhibition of the non-specific degradation of ZnO NPs

To investigate whether the mesoporous silica shell could protect the ZnO-DOX complex from non-specific degradation caused by protein, and thus retain its pH-responsiveness, BSA was chosen as a model

protein to interact with ZnO-DOX and ZnO-DOX@F-mSiO$_2$-FA NPs, respectively. The dissolved zinc ion concentration was determined by ICP-MS. As shown in Table S1 (in the ESM), the mass of zinc from the group containing ZnO-DOX and BSA (pH 7.4) was 10 times higher than that from the control group (pH 7.4), which showed that protein promoted the degradation of ZnO-DOX NPs. The mass of zinc from ZnO-DOX@F-mSiO$_2$-FA was significantly lower than that from ZnO-DOX under the same treatment, which suggested that the mesoporous silica shell protected ZnO-DOX from non-specific degradation. The structural changes of ZnO-DOX@F-mSiO$_2$-FA NPs were further characterized using TEM. Figure S5 in the ESM suggested that the ZnO-DOX NPs became irregular and wrinkled when treated with BSA. More importantly, as shown in Fig. 1(b), the core–shell structure of ZnO-DOX@F-mSiO$_2$-FA NPs treated with BSA remained intact and appeared similar to those of the control group (pH 7.4). However, the interior of the ZnO-DOX@F-mSiO$_2$-FA NPs in acetate buffer at pH 4.5 was empty. These results indicated that the mesoporous silica shell could prevent protein-induced degradation effectively and maintained the pH responsiveness of the NPs.

3.3 Targeting ability of pH-sensitive nanoreactors

To evaluate the tumor-targeting ability of our designed nanoreactors, a human cervical epithelial carcinoma cell line (HeLa, folate receptor (FR)-positive) and a human embryonic kidney fibroblast cell line (HEK 293T, FR-negative) were chosen as model cells. Both DOX-unloaded NPs (ZnO@F-mSiO$_2$-FA, Fig. S6(a) in the ESM) and ZnO-DOX@F-mSiO$_2$-FA were treated with HeLa cells and HEK 293T cells, respectively. The results of flow cytometry analysis (Fig. S6(b) in the ESM) showed a large shift for HeLa cells treated with the ZnO-DOX@F-mSiO$_2$-FA and ZnO@F-mSiO$_2$-FA NPs. In contrast, neither the shift nor enhancement was observed for HEK 293T cells using the same treatments. A co-localization study was further carried out to determine if our designed NPs could accumulate within the lysosomes and endosomes after endocytosis. As shown in Fig. S6(c) (in the ESM), the green fluorescence of FITC was apparent within HeLa cells and co-localized with the lysotracker red fluorescence, implying that the FITC-labeled NPs had become highly concentrated within the endosomes and lysosomes of the HeLa cells. No significant green fluorescence was observed in HEK 293T cells under the same treatments. These results verified the tumor-targeting ability of our designed pH-sensitive nanoreactors. The targeted drug delivery ability could be attributed to the special interaction between FA and the FR, which is overexpressed on the surface of HeLa cells.

3.4 Monitoring and visualizing drug release behavior

To assess the controllable drug-releasing behavior,

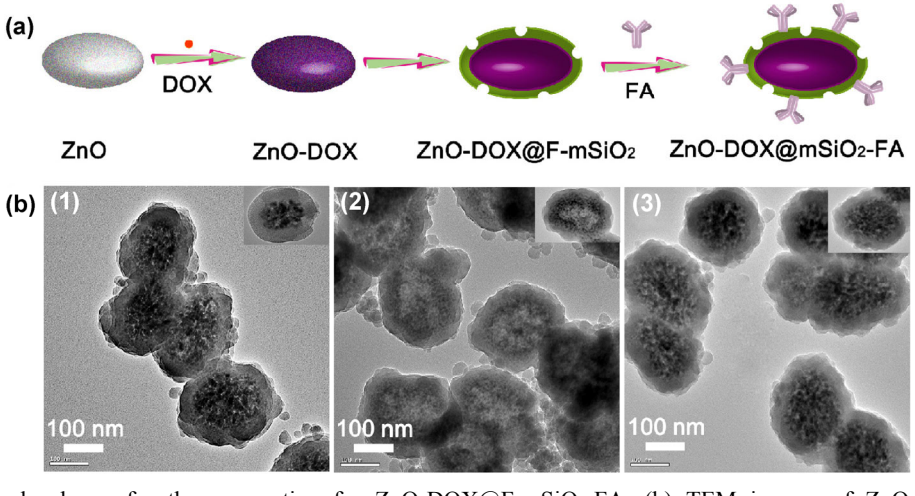

Figure 1 (a) General scheme for the preparation for ZnO-DOX@F-mSiO$_2$-FA. (b) TEM images of ZnO-DOX@F-mSiO$_2$-FA nanoparticles with different treatments: (1) pH 7.4 PBS; (2) pH 4.5 acetic acid; (3) pH 7.4 PBS plus BSA.

leakage tests were first carried out. Figure S7 in the ESM shows that no DOX leached out of the NPs on exposure to cell culture medium over 48 h. Next, the DOX releasing profiles were investigated at different pH values. As shown in Fig. S8 (in the ESM), the release of DOX from ZnO-DOX@F-mSiO$_2$-FA NPs was negligible under physiological conditions (pH 7.4) within 12 h, even in the presence of protein. In contrast, in an acid environment (pH 4.5), up to 90% of DOX was released from ZnO-DOX@F-mSiO$_2$-FA NPs within 3 h, because of the degradation of the ZnO NPs. Therefore, these results demonstrated that our designed nanoreactors could respond to changing pH values to control DOX release, even in the presence of protein.

To confirm that the DOX release behavior could be monitored using two different fluorescent molecules, ZnO-DOX@F-mSiO$_2$-FA NPs were treated with PBS at different pH values. The supernatant and precipitate were then characterized by fluorescence spectroscopy. As shown in Fig. 2(b), the supernatant at pH 4.5 showed the characteristic fluorescent emission of DOX. Similarly, the redissolved precipitate (F-mSiO$_2$) at pH 4.5 exhibited stronger FITC fluorescence than that at pH 7.4. These results could be explained as follows. At pH 7.4, ZnO-DOX could quench the fluorescence of F-mSiO$_2$ (Fig. S9 in the ESM). At pH 4.5, the degradation of ZnO NPs resulted in the recovery of green fluorescence from F-mSiO$_2$ and the release of DOX from the ZnO-DOX complex. The DOX release behavior was visualized directly using a fluorescent microscope (Fig. S10 in the ESM), and was consistent with the corresponding fluorescence spectrum. In PBS (pH 7.4), the red fluorescence of DOX and the green fluorescence from F-mSiO$_2$ were both weaker. By contrast, at pH 4.5, both the red fluorescence from DOX and the green fluorescence from F-mSiO$_2$ increased because of the degradation of ZnO NPs. These results encouraged us to examine whether this system could work in cells.

Next, HeLa cells were treated with free DOX and ZnO-DOX@F-mSiO$_2$-FA for 4 h, respectively, and its subcellular locations were observed using a CLSM (Fig. 2(b)). As shown in the fluorescent images of free

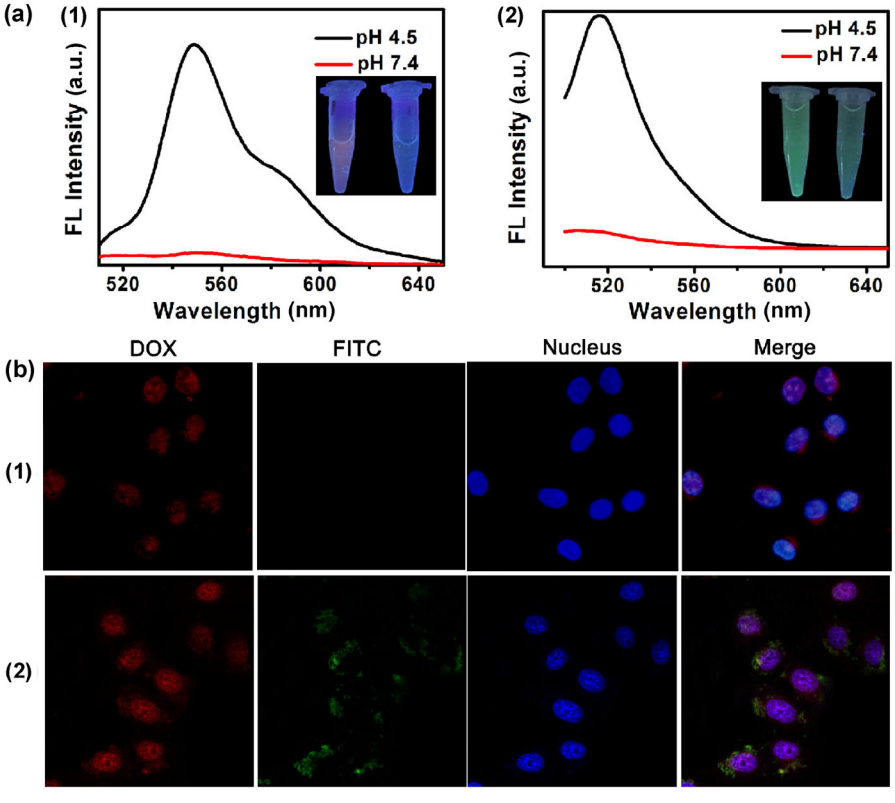

Figure 2 (a) Fluorescence spectra and the corresponding photographs of (1) supernatant and (2) precipitate after dissolution. (b) Spatial distribution of (1) free DOX and (2) ZnO-DOX@F-mSiO$_2$-FA nanoparticles in HeLa cells.

DOX, the red fluorescence of DOX was clearly visible in the cell nuclei, where it could execute its anti-cancer functions. As for ZnO-DOX@F-mSiO$_2$-FA NPs, the red fluorescence of DOX appeared in the cell nuclei at the same position as free DOX. Moreover, the fluorescence intensity of DOX from the NPs was much stronger than that of free DOX, which suggested that this pH nanoreactor could deliver DOX into cells more effectively. The green fluorescence of F-mSiO$_2$ was observed mostly in the cytoplasm, not in the nucleus. These results also indicated that ZnO-DOX@F-mSiO$_2$-FA NPs were first taken up by HeLa cells, and then, DOX was released from the ZnO-DOX@F-mSiO$_2$-FA NPs. Meanwhile, the drug release behavior could be monitored via the fluorescence from FITC and DOX.

3.5 Cell viability assay

A standard methyl thiazolyl tetrazolium (MTT) assay was used to assess the cell viability. Growth inhibition of cells was observed after incubation with free DOX, ZnO, ZnO-DOX, and non-fluorescent silica nanoreactors (ZnO@mSiO$_2$-FA and ZnO-DOX@mSiO$_2$-FA, Scheme S1), respectively. As shown in Fig. S11 (in the ESM), DOX, ZnO, and ZnO-DOX showed similar cytotoxicity. In contrast, ZnO@mSiO$_2$-FA and ZnO-DOX@mSiO$_2$-FA had obviously different killing efficiencies on HEK 293T and HeLa cells. They exhibited negligible cytotoxicity toward HEK 293T cells. However, for HeLa cells, they exhibited dose-dependent anticancer behavior. Interestingly, at each concentration, ZnO-DOX@mSiO$_2$-FA showed higher cytotoxicity than free DOX and ZnO@mSiO$_2$-FA NPs alone. We speculated that the enhanced anti-cancer efficiency was due to the synergetic effect of the nanoparticle-induced oxidative stress and anticancer drug [58, 59].

3.6 Possible mechanism of pH-sensitive nanoreactors as anti-cancer agents

To verify whether our designed nanoreactors could produce zinc ions and ROS to enhance the therapeutic effect, the non-fluorescent ZnO@mSiO$_2$-FA NPs were incubated with HeLa cells and HEK 293T cells, respectively. First, zinquin ethyl ester, which is a zinc ion-sensitive blue fluorescent probe, was used to survey the intracellular biodegradation of the pH-sensitive nanoreactor. As shown in Fig. 3(a), weak blue fluore-

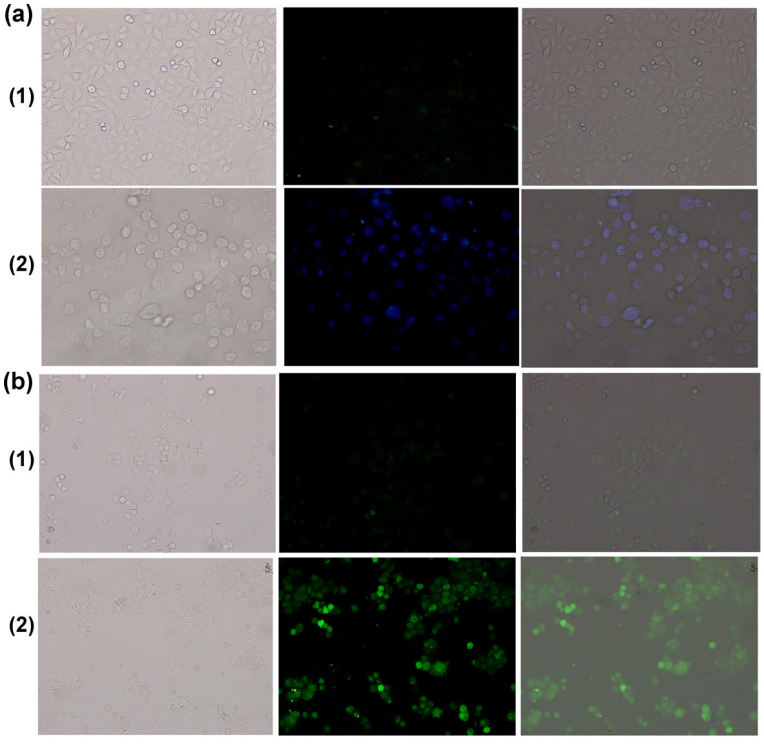

Figure 3 (a) Zinc ions and (b) ROS detection in HeLa cells under different treatments: (1) control; (2) ZnO@mSiO$_2$-FA. Zinc ions were stained by a zinquin ethyl ester blue fluorescent probe and ROS were traced by DCFH-DA.

scence was observed in HeLa cells of the control group because of the trace amount of zinc included in the cell culture medium. As expected, significantly enhanced blue fluorescence was observed when the HeLa cells were treated with ZnO@mSiO$_2$-FA. However, no obvious blue fluorescence was observed in HEK 293T cells treated with ZnO@mSiO$_2$-FA or in non-treated controls (Fig. S12(a) in the ESM). The results suggested that ZnO@mSiO$_2$-FA was degraded and generated zinc ions in the target cancer cells. Second, since ROS could oxidize dichlorofluorescin diacetate (DCFH-DA) to produce dichlorofluorescin (DCF, a green fluorescent probe), DCFH-DA could be used to substantiate the intracellular ROS produced by ZnO@mSiO$_2$-FA NPs. As shown in Fig. 3(b), strong green fluorescence was observed when HeLa cells were treated with ZnO@mSiO$_2$-FA, indicating the production of intracellular ROS. However, green fluorescence was not observed in HEK 293T cells under the same treatment (Fig. S12(b) in the ESM). Meanwhile, flow cytometry was used to quantify the intracellular ROS. A significant shift was observed when HeLa cells were treated with ZnO@mSiO$_2$-FA, whereas no obvious difference was observed for HEK 293T cells, whether treated with ZnO@mSiO$_2$-FA or not (Fig. S13 in the ESM). Taken together, the results demonstrated that the intracellular biodegradation of the pH-sensitive nanoreactors would produce zinc ions and ROS to enhance cancer treatment.

To determine possible mechanism of cell death,

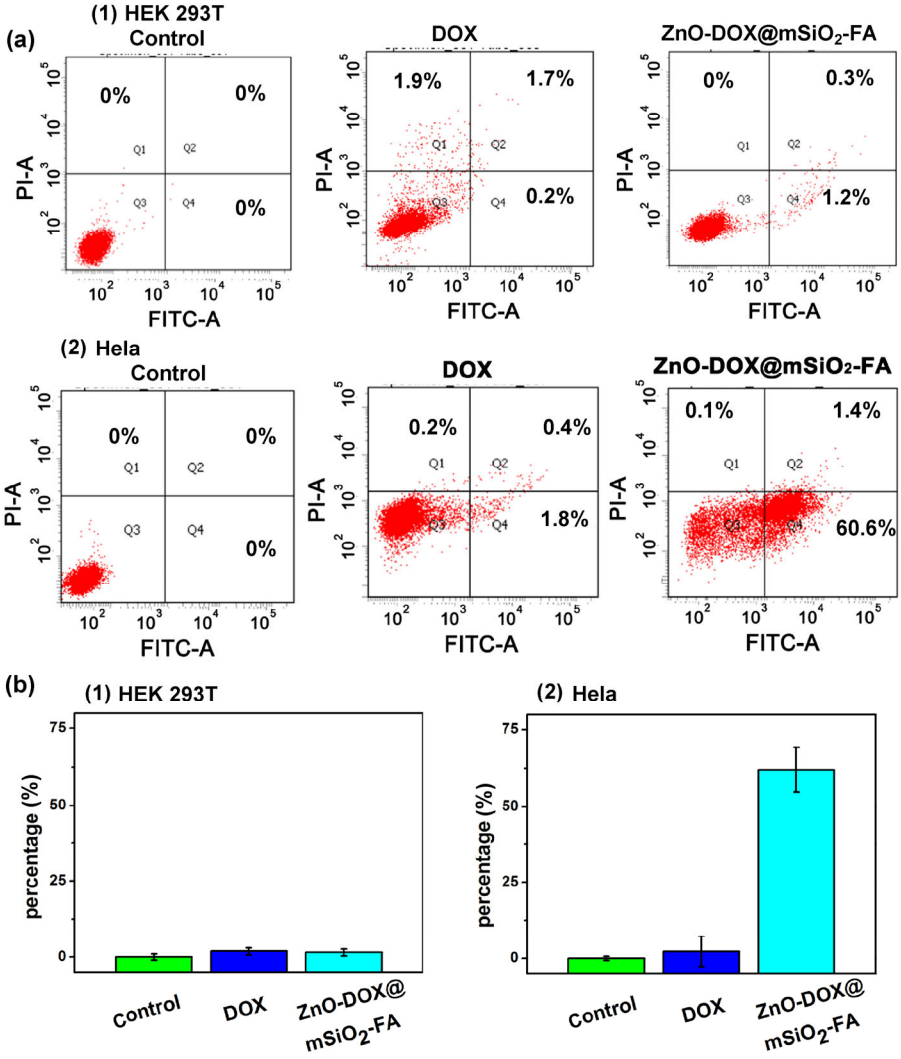

Figure 4 (a) Flow cytometry representing an apoptosis assay-based annexin V-FITC and PI staining and (b) the corresponding percentage of cell apoptosis. (1) HEK 293T cells and (2) HeLa cells were treated with control, free DOX, and ZnO-DOX@mSiO$_2$-FA, respectively.

a propidium iodide (PI) and annexin V-fluorescein isothiocyanate (annexin V-FITC) staining assay and flow cytometry were used. Early apoptotic cells and live cells cannot be labeled by PI, whereas apoptotic cells could be identified by annexin V-FITC. As shown in Fig. 4, free DOX could not induce significant death of both kinds of cells within 12 h, which was consistent with the MTT results. In contrast, ZnO-DOX@mSiO$_2$-FA showed specific cytotoxicity toward HeLa cells and no significant toxicity toward HEK 293T cells, indicating the targeting effect. Notably, after treatment with ZnO-DOX@mSiO$_2$-FA, a remarkably higher proportion of HeLa cells was annexin V-FITC positive compared with those of the control and DOX alone groups. This indicated that our designed ZnO-DOX@mSiO$_2$-FA could enhance apoptosis of HeLa cells.

Based on the aforementioned results, our designed nanoreactors were first taken up by cancer cells via a passive enhanced permeability and retention (EPR) effect, together with active targeting effect (Fig. 5). Subsequently, they were transported into acidic endo/lysosomes and rapidly biodegraded to generate cytotoxic zinc ions and destructive ROS. This would help DOX to escape from the lysosome, and enter and mark the cell nucleus. Our designed nanoreactor has three possible advantages: i) The degradation of ZnO only happens in organelles with a low internal pH such as lysosomes, avoiding non-specific degradation effectively; ii) the pH-sensitive nanoreactor could produce synergetic therapy of nanoparticle-induced oxidative stress and the chemotherapeutic agent; and iii) multifunctional platforms to control and visualize the release of anticancer drugs have been integrated into one system.

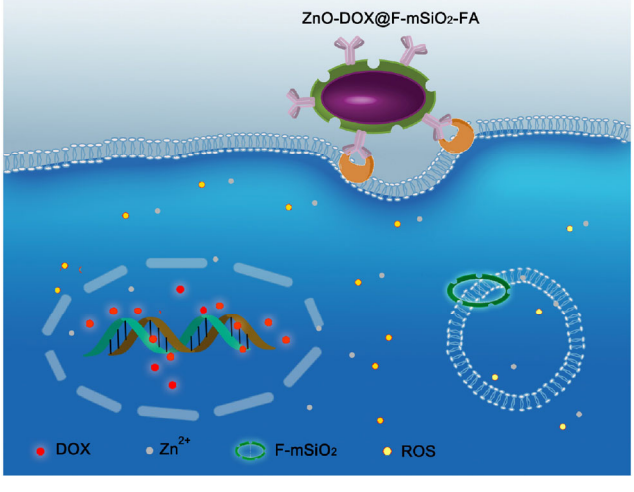

Figure 5 Schematic illustration of the pH-sensitive mesoporous silica nanoreactor used for targeted anticancer treatment.

4 Conclusions

In summary, we have developed a pH-sensitive nanoreactor that can release cytotoxic zinc ions, ROS, and anticancer drugs efficiently in response to an acidic microenvironment, thereby causing apoptosis of the targeted cancer cells. This work may promote the development of new types of mesoporous nanoreactors for cancer diagnosis and treatment.

Acknowledgements

This work was supported by the National Basic Research Program of China (No. 2012CB720602) and the National Natural Science Foundation of China (Nos. 21210002, 21431007, and 21533008).

Electronic Supplementary Material: Supplementary material (further details of TEM images, UV–Vis measurements, zinc ions and ROS detection, and MTT results) is available in the online version of this article at http://dx.doi.org/10.1007/s12274-016-1377-2.

References

[1] Petros, R. A.; DeSimone, J. M. Strategies in the design of nanoparticles for therapeutic applications. *Nat. Rev. Drug Discov.* **2010**, *9*, 615–627.

[2] Lee, J. H.; Yigit, M. V.; Mazumdar, D.; Lu, Y. Molecular diagnostic and drug delivery agents based on aptamer-nanomaterial conjugates. *Adv. Drug Deliv. Rev.* **2010**, *62*, 592–605.

[3] Caldorera-Moore, M. E.; Liechty, W. B.; Peppas, N. A. Responsive theranostic systems: Integration of diagnostic imaging agents and responsive controlled release drug delivery carriers. *Acc. Chem. Res.* **2011**, *44*, 1061–1070.

[4] Doane, T. L.; Burda, C. The unique role of nanoparticles in nanomedicine: Imaging, drug delivery and therapy. *Chem. Soc. Rev.* **2012**, *41*, 2885–2911.

[5] Li, Z. X.; Barnes, J. C.; Bosoy, A.; Stoddart, J. F.; Zink, J. I.

Mesoporous silica nanoparticles in biomedical applications. *Chem. Soc. Rev.* **2012**, *41*, 2590–2605.

[6] Casasús, R.; Climent, E.; Marcos, M. D.; Martínez-Máñez, R.; Sancenón, F.; Soto, J.; Amorós, P.; Cano, J.; Ruiz, E. Dual aperture control on pH- and anion-driven supramolecular nanoscopic hybrid gate-like ensembles. *J. Am. Chem. Soc.* **2008**, *130*, 1903–1917.

[7] Aznar, E.; Marcos, M. D.; Martínez-Máñez, R.; Sancenón, F.; Soto, J.; Amorós, P.; Guillem, C. pH- and photo-switched release of guest molecules from mesoporous silica supports. *J. Am. Chem. Soc.* **2009**, *131*, 6833–6843.

[8] Ferris, D. P.; Zhao, Y.-L.; Khashab, N. M.; Khatib, H. A.; Stoddart, J. F.; Zink, J. I. Light-operated mechanized nanoparticles. *J. Am. Chem. Soc.* **2009**, *131*, 1686–1688.

[9] Chen, C. E.; Geng, J.; Pu, F.; Yang, X. J.; Ren, J. S.; Qu, X. G. Polyvalent nucleic acid/mesoporous silica nanoparticle conjugates: Dual stimuli-responsive vehicles for intracellular drug delivery. *Angew. Chem., Int. Ed.* **2011**, *50*, 882–886.

[10] Shi, P.; Li, M.; Ren, J. S.; Qu, X. G. Gold nanocage-based dual responsive "caged metal chelator" release system: Noninvasive remote control with near infrared for potential treatment of Alzheimer's disease. *Adv. Funct. Mater.* **2013**, *23*, 5412–5419.

[11] Chen, Z. W.; Li, Z. H.; Lin, Y. H.; Yin, M. L.; Ren, J. S.; Qu, X. G. Biomineralization inspired surface engineering of nanocarriers for pH-responsive, targeted drug delivery. *Biomaterials* **2013**, *34*, 1364–1371.

[12] Chung, M. F.; Liu, H. Y.; Lin, K. J.; Chia, W. T.; Sung, H. W. A pH-responsive carrier system that generates NO bubbles to trigger drug release and reverse P-glycoprotein-mediated multidrug resistance. *Angew. Chem., Int. Ed.* **2015**, *54*, 9890–9893.

[13] Kim, B. J.; Cheong, H.; Hwang, B. H.; Cha, H. J. Mussel-inspired protein nanoparticles containing iron(III)-DOPA complexes for pH-responsive drug delivery. *Angew. Chem., Int. Ed.* **2015**, *54*, 7318–7322.

[14] Liu, R.; Zhang, Y.; Zhao, X.; Agarwal, A.; Mueller, L. J.; Feng, P. Y. pH-responsive nanogated ensemble based on gold-capped mesoporous silica through an acid-labile acetal linker. *J. Am. Chem. Soc.* **2010**, *132*, 1500–1501.

[15] Xiong, H.-M.; Xu, Y.; Ren, Q.-G.; Xia, Y.-Y. Stable aqueous ZnO@polymer core−shell nanoparticles with tunable photoluminescence and their application in cell imaging. *J. Am. Chem. Soc.* **2008**, *130*, 7522–7523.

[16] Muhammad, F.; Guo, M. Y.; Guo, Y. J.; Qi, W. X.; Qu, F. Y.; Sun, F. X.; Zhao, H. J.; Zhu, G. S. Acid degradable ZnO quantum dots as a platform for targeted delivery of an anticancer drug. *J. Mater. Chem.* **2011**, *21*, 13406–13412.

[17] Muhammad, F.; Guo, M. Y.; Qi, W. X.; Sun, F. X.; Wang, A. F.; Guo, Y. J.; Zhu, G. S. pH-triggered controlled drug release from mesoporous silica nanoparticles via intracelluar dissolution of ZnO nanolids. *J. Am. Chem. Soc.* **2011**, *133*, 8778–8781.

[18] Xiong, H. M. ZnO nanoparticles applied to bioimaging and drug delivery. *Adv. Mater.* **2013**, *25*, 5329–5335.

[19] Wang, Y. H.; Song, S. Y.; Liu, J. H.; Liu, D. P.; Zhang, H. J. ZnO-functionalized upconverting nanotheranostic agent: Multi-modality imaging-guided chemotherapy with on-demand drug release triggered by pH. *Angew. Chem., Int. Ed.* **2015**, *54*, 536–540.

[20] Zhang, J.; Wu, D.; Li, M. F.; Feng, J. Multifunctional mesoporous silica nanoparticles based on charge-reversal plug-gate nanovalves and acid-decomposable ZnO quantum dots for intracellular drug delivery. *ACS Appl. Mater. Interfaces* **2015**, *7*, 26666–26673.

[21] Applerot, G.; Lipovsky, A.; Dror, R.; Perkas, N.; Nitzan, Y.; Lubart, R.; Gedanken, A. Enhanced antibacterial activity of nanocrystalline ZnO due to increased ROS-mediated cell injury. *Adv. Funct. Mater.* **2009**, *19*, 842–852.

[22] Xu, M. S.; Li, J.; Hanagata, N.; Su, H. X.; Chen, H. Z.; Fujita, D. Challenge to assess the toxic contribution of metal cation released from nanomaterials for nanotoxicology-the case of ZnO nanoparticle. *Nanoscale* **2013**, *5*, 4763–4769.

[23] Chen, Z. W.; Li, Z. H.; Wang, J. S.; Ju, E. G.; Zhou, L.; Ren, J. S.; Qu, X. G. A multi-synergistic platform for sequential irradiation-activated high-performance apoptotic cancer therapy. *Adv. Funct. Mater.* **2014**, *24*, 522–529.

[24] Gupta, J.; Bhargava, P.; Bahadur, D. Fluorescent ZnO for imaging and induction of DNA fragmentation and ROS-mediated apoptosis in cancer cells. *J. Mater. Chem. B* **2015**, *3*, 1968–1978.

[25] Chen, W. H.; Luo, G. F.; Qiu, W. X.; Lei, Q.; Hong, S.; Wang, S. B.; Zheng, D. W.; Zhu, C. H.; Zeng, X.; Feng, J. et al. Programmed nanococktail for intracellular cascade reaction regulating self-synergistic tumor targeting therapy. *Small* **2016**, *12*, 733–744.

[26] Barick, K. C.; Nigam, S.; Bahadur, D. Nanoscale assembly of mesoporous ZnO: A potential drug carrier. *J. Mater. Chem.* **2010**, *20*, 6446–6452.

[27] Mitra, S.; Subia, B.; Patra, P.; Chandra, S.; Debnath, N.; Das, S.; Banerjee, R.; Kundu, S. C.; Pramanik, P.; Goswami, A. Porous ZnO nanorod for targeted delivery of doxorubicin: *In vitro* and *in vivo* response for therapeutic applications. *J. Mater. Chem.* **2012**, *22*, 24145–24154.

[28] Zhang, Z. Y.; Xu, Y. D.; Ma, Y. Y.; Qiu, L. L.; Wang, Y.; Kong, J. L.; Xiong, H. M. Biodegradable ZnO@polymer core–shell nanocarriers: pH-triggered release of doxorubicin *in vitro*. *Angew. Chem., Int. Ed.* **2013**, *52*, 4127–4131.

[29] Moreau, J. W.; Weber, P. K.; Martin, M. C.; Gilbert, B.; Hutcheon, I. D.; Banfield, J. F. Extracellular proteins limit the dispersal of biogenic nanoparticles. *Science* **2007**, *316*, 1600–1603.

[30] Xia, T.; Kovochich, M.; Liong, M.; Mädler, L.; Gilbert, B.; Shi, H. B.; Yeh, J. I.; Zink, J. I.; Nel, A. E. Comparison of the mechanism of toxicity of zinc oxide and cerium oxide nanoparticles based on dissolution and oxidative stress properties. *ACS Nano* **2008**, *2*, 2121–2134.

[31] Nel, A. E.; Mädler, L.; Velegol, D.; Xia, T.; Hoek, E. M. V.; Somasundaran, P.; Klaessig, F.; Castranova, V.; Thompson, M. Understanding biophysicochemical interactions at the nano-bio interface. *Nat. Mater.* **2009**, *8*, 543–557.

[32] Müller, K. H.; Kulkarni, J.; Motskin, M.; Goode, A.; Winship, P.; Skepper, J. N.; Ryan, M. P.; Porter, A. E. pH-dependent toxicity of high aspect ratio ZnO nanowires in macrophages due to intracellular dissolution. *ACS Nano* **2010**, *4*, 6767–6779.

[33] George, S.; Pokhrel, S.; Xia, T.; Gilbert, B.; Ji, Z. X.; Schowalter, M.; Rosenauer, A.; Damoiseaux, R.; Bradley, K. A.; Mädler, L. et al. Use of a rapid cytotoxicity screening approach to engineer a safer zinc oxide nanoparticle through iron doping. *ACS Nano* **2010**, *4*, 15–29.

[34] Luo, M. D.; Shen, C. C.; Feltis, B. N.; Martin, L. L.; Hughes, A. E.; Wright, P. F. A.; Turney, T. W. Reducing ZnO nanoparticle cytotoxicity by surface modification. *Nanoscale* **2014**, *6*, 5791–5798.

[35] Zhao, Y.; Luo, Z.; Li, M. H.; Qu, Q. Y.; Ma, X.; Yu, S. H.; Zhao, Y. L. A preloaded amorphous calcium carbonate/doxorubicin@silica nanoreactor for pH-responsive delivery of an anticancer drug. *Angew. Chem., Int. Ed.* **2015**, *54*, 919–922.

[36] Vázquez-Vázquez, C.; Vaz, B.; Giannini, V.; Pérez-Lorenzo, M.; Alvarez-Puebla, R. A.; Correa-Duarte, M. A. Nanoreactors for simultaneous remote thermal activation and optical monitoring of chemical reactions. *J. Am. Chem. Soc.* **2013**, *135*, 13616–13619.

[37] Huang, Y. Y.; Lin, Y. H.; Ran, X.; Ren, J. S.; Qu, X. G. Self-assembly and compartmentalization of nanozymes in mesoporous silica-based nanoreactors. *Chem.—Eur. J.* **2016**, *22*, 5705–5711.

[38] Min, Q. B.; Wu, R. A.; Zhao, L.; Qin, H. Q.; Ye, M. L.; Zhu, J. J.; Zou, H. F. Size-selective proteolysis on mesoporous silica-based trypsin nanoreactor for low-MW proteome analysis. *Chem. Commun.* **010**, *46*, 6144–6146.

[39] Hu, J.; Chen, M.; Fang, X. S.; Wu, L. M. Fabrication and application of inorganic hollow spheres. *Chem. Soc. Rev.* **2011**, *40*, 5472–5491.

[40] Choi, E.; Kwak, M.; Jang, B.; Piao, Y. Z. Highly monodisperse rattle-structured nanomaterials with gold nanorod core-mesoporous silica shell as drug delivery vehicles and nanoreactors. *Nanoscale* **2013**, *5*, 151–154.

[41] Kim, S. M.; Jeon, M.; Kim, K. W.; Park, J.; Lee, I. S. Postsynthetic functionalization of a hollow silica nanoreactor with manganese oxide-immobilized metal nanocrystals inside the cavity. *J. Am. Chem. Soc.* **2013**, *135*, 15714–15717.

[42] Xu, H. J.; Zhang, H. J.; Wang, D. H.; Wu, L.; Liu, X. W.; Jiao, Z. A facile route for rapid synthesis of hollow mesoporous silica nanoparticles as pH-responsive delivery carrier. *J. Colloid Interface Sci.* **2015**, *451*, 101–107.

[43] Guerrero-Martínez, A.; Pérez-Juste, J.; Liz-Marzán, L. M. Recent progress on silica coating of nanoparticles and related nanomaterials. *Adv. Mater.* **2010**, *22*, 1182–1195.

[44] Zhai, J.; Tao, X.; Pu, Y.; Zeng, X.-F.; Chen, J.-F. Core/shell structured ZnO/SiO_2 nanoparticles: Preparation, characterization and photocatalytic property. *Appl. Surf. Sci.* **2010**, *257*, 393–397.

[45] Zhao, Y.; Lin, L. N.; Lu, Y.; Chen, S. F.; Dong, L.; Yu, S. H. Templating synthesis of preloaded doxorubicin in hollow mesoporous silica nanospheres for biomedical applications. *Adv. Mater.* **2010**, *22*, 5255–5259.

[46] Liu, J.; Qiao, S. Z.; Hu, Q. H.; Lu, G. Q. Magnetic nanocomposites with mesoporous structures: Synthesis and applications. *Small* **2011**, *7*, 425–443.

[47] Liu, J.; Bu, J. W.; Bu, W. B.; Zhang, S. J.; Pan, L. M.; Fan, W. P.; Chen, F.; Zhou, L. P.; Peng, W. J.; Zhao, K. L. et al. Real-time *in vivo* quantitative monitoring of drug release by dual-mode magnetic resonance and upconverted luminescence imaging. *Angew. Chem., Int. Ed.* **2014**, *53*, 4551–4555.

[48] Fan, W. P.; Shen, B.; Bu, W. B.; Chen, F.; Zhao, K. L.; Zhang, S. J.; Zhou, L. P.; Peng, W. J.; Xiao, Q. F.; Xing, H. Y. et al. Rattle-structured multifunctional nanotheranostics for synergetic chemo-/radiotherapy and simultaneous magnetic/luminescent dual-mode imaging. *J. Am. Chem. Soc.* **2013**, *135*, 6494–6503.

[49] Yoon, T. J.; Kim, J. S.; Kim, B. G.; Yu, K. N.; Cho, M. H.; Lee, J. K. Multifunctional nanoparticles possessing a "magnetic motor effect" for drug or gene delivery. *Angew. Chem., Int. Ed.* **2005**, *44*, 1068–1071.

[50] Liong, M.; Lu, J.; Kovochich, M.; Xia, T.; Ruehm, S. G.; Nel, A. E.; Tamanoi, F.; Zink, J. I. Multifunctional inorganic nanoparticles for imaging, targeting, and drug delivery. *ACS Nano* **2008**, *2*, 889–896.

[51] Shi, P.; Liu, Z.; Dong, K.; Ju, E. G.; Ren, J. S.; Du, Y. D.; Li, Z. Q.; Qu, X. G. A smart "sense-act-treat" system: Combining a ratiometric pH sensor with a near infrared therapeutic gold nanocage. *Adv. Mater.* **2014**, *26*, 6635–6641.

[52] Chen, T. T.; Hu, Y. H.; Cen, Y.; Chu, X.; Lu, Y. A dual-emission fluorescent nanocomplex of gold-cluster-decorated

silica particles for live cell imaging of highly reactive oxygen species. *J. Am. Chem. Soc.* **2013**, *135*, 11595–11602.

[53] Xue, X. D.; Zhao, Y. Y.; Dai, L. R.; Zhang, X.; Hao, X. H.; Zhang, C. Q.; Huo, S. D.; Liu, J.; Liu, C.; Kumar, A. et al. Spatiotemporal drug release visualized through a drug delivery system with tunable aggregation-induced emission. *Adv. Mater.* **2014**, *26*, 712–717.

[54] Yan, Z. Q.; Shi, P.; Ren, J. S.; Qu, X. G. A "sense-and-treat" hydrogel used for treatment of bacterial infection on the solid matrix. *Small* **2015**, *11*, 5540–5544.

[55] Deng, X. Y.; Luan, Q. X.; Chen, W. T.; Wang, Y. L.; Wu, M. H.; Zhang, H. J.; Jiao, Z. Nanosized zinc oxide particles induce neural stem cell apoptosis. *Nanotechnology* **2009**, *20*, 115101.

[56] Narayanan, S.; Binulal, N. S.; Mony, U.; Manzoor, K.; Nair, S.; Menon, D. Folate targeted polymeric "green" nanotherapy for cancer. *Nanotechnology* **2010**, *21*, 285107.

[57] Li, Z. H.; Dong, K.; Huang, S.; Ju, E. G.; Liu, Z.; Yin, M. L.; Ren, J. S.; Qu, X. G. A smart nanoassembly for multistage targeted drug delivery and magnetic resonance imaging. *Adv. Funct. Mater.* **2014**, *24*, 3612–3620.

[58] Conte, C.; Ungaro, F.; Maglio, G.; Tirino, P.; Siracusano, G.; Sciortino, M. T.; Leone, N.; Palma, G.; Barbieri, A.; Arra, C. et al. Biodegradable core–shell nanoassemblies for the delivery of docetaxel and Zn(II)-phthalocyanine inspired by combination therapy for cancer. *J. Control. Release* **2013**, *167*, 40–52.

[59] Miao, W. J.; Shim, G.; Lee, S.; Lee, S.; Choe, Y. S.; Oh, Y. K. Safety and tumor tissue accumulation of pegylated graphene oxide nanosheets for co-delivery of anticancer drug and photosensitizer. *Biomaterials* **2013**, *34*, 3402–3410.